JOURNAL OF GEOPHYSICAL RESEARCH, VOL. 92, NO. A1, PAGES 127–142, JANUARY 1, 1987

Gyroresonant Pitch Angle Scattering by Coherent and Incoherent Whistler Mode Waves in the Magnetosphere

UMRAN S. INAN

STAR Laboratory, Stanford University, Stanford, California

A test particle approach is used to compare gyroresonant pitch angle scattering of energetic electrons by coherent versus incoherent whistler mode waves, for the case in which the coherent wave amplitude is below the nonlinear phase trapping threshold. Wave packets of 400 ms duration propagating along the magnetic field at $L = 4$ within the plasmasphere are considered, and the wave-induced pitch angle scattering along the propagation path from one hemisphere to the other and the resulting precipitation flux are computed. An incoherent wave spectrum is simulated by random modulation of the wave frequency at intervals of 1 ms, thereby generating signals with nearly constant power spectral density over a bandwidth of 2 kHz centered at 5.5 kHz. The associated pitch angle scattering is compared with that of a monochromatic 5.5-kHz signal of 400 ms duration. Results of the test particle analysis are compared with those expected on the basis of a classical diffusion treatment, and an expression is derived for an effective "diffusion" coefficient for pitch angle scattering by coherent waves. The trajectory followed by a particle when interacting with incoherent waves essentially represents a random walk in velocity space, while for coherent waves the pitch angle of the particle varies in a well-defined manner. In spite of the fact that individual particle scatterings are typically larger for coherent waves, the peak precipitation fluxes induced by incoherent waves are found to be approximately the same as those for coherent waves having the same total power. This results from the fact that incoherent waves interact with particles over a wider range of energies. As a consequence, the energy spectrum and the temporal extent of transient precipitation pulses due to incoherent wave packets are broader than those for equivalent coherent ones.

1. INTRODUCTION

An important consequence of wave-particle interactions in planetary magnetospheres is the pitch angle scattering of trapped energetic particles, resulting in the perturbation of the stable orbits of the same particles and their precipitation into the denser lower atmosphere. Magnetospheric waves may arise from a variety of sources [*Shawhan*, 1979]. In the inner magnetosphere on primarily closed field lines ($L \leq 6$), and for interactions with energetic (100 eV to 1 MeV) electrons, waves propagating in the whistler mode [*Helliwell*, 1965] have been extensively studied, and are believed to be important in the loss of the trapped particles and thus in limiting the trapped particle flux levels [*Brice*, 1964; *Kennel and Petschek*, 1966; *Lyons et al.*, 1972]. Whistler-mode waves propagate at frequencies between the proton and electron gyrofrequencies, and exhibit spectral power near the natural gyration frequency in the frame of the electron's adiabatic motion. Thus, these waves perturb the adiabatic invariant motion of the particles, and the wave-induced pitch angle and energy changes can result in the lowering of the "mirror" altitude of the particles, and the precipitation of the electrons into the ionosphere.

Examples of whistler mode waves in the inner magnetosphere include (1) lightning generated whistlers, (2) spontaneous natural emissions such as ELF/VLF hiss and chorus, (3) man-made waves from VLF transmitters and large power grids, and (4) emissions triggered by either whistlers and/or man-made waves. While all of these waves have been extensively observed on the ground and on satellites, their relative importance in contributing to the loss of radiation belt particles is still not known. The possible role of lightning-generated whistlers in precipitating radiation belt electrons was suggested shortly after the discovery of the radiation belts [*Dungey*, 1963; *Cornwall*, 1964]. Later work was concentrated on pitch angle scattering induced by incoherent signals [*Roberts*, 1969] and plasmaspheric hiss was suggested as the dominant cause of the loss of particles within the plasmasphere [*Lyons et al.*, 1972]. More recent findings involve whistler-induced electron precipitation, in terms of indirect ground-based observations [*Helliwell et al.*, 1973; *Lohrey and Kaiser*, 1979; *Carpenter and LaBelle*, 1982; *Leyser et al.*, 1984; *Inan et al.*, 1985*b*], as well as direct observations on satellites and rockets [*Rycroft*, 1973; *Voss et al.*, 1984; *Goldberg et al.*, 1985]. This work has provided striking new evidence of the removal of electrons from the radiation belts by lightning-generated whistlers, especially at middle to low latitudes ($L \leq 3$), and has thus stimulated new interest in the role of whistlers in the dynamics of the radiation belt particles. At higher latitudes, outside the plasmasphere, VLF chorus emissions and whistler-triggered emissions are known to produce detectable precipitation fluxes [*Rosenberg et al.*, 1971; *Helliwell et al.*, 1980]. However, the effect of chorus or whistler-induced precipitation on the overall loss rates of trapped electrons, and the relative effects of these versus other waves remain to be determined.

In the past two decades, considerable work has been done on pitch angle scattering of radiation belt particles by waves [*Roberts*, 1966, 1968, 1969; *Cornwall*, 1966; *Cornwall and Cocke*, 1967; *Gendrin*, 1968; *Kennel and Petschek*, 1966; *Ashour-Abdalla*, 1972; *Lyons*, 1973; 1974; *Lyons et al.*, 1971, 1972; *Schulz and Lanzerotti*, 1974]. All of this early work, however, has addressed the problem of scattering by wide-band incoherent whistler-mode or hydromagnetic turbulence, with the exception of *Ashour-Abdalla* [1972] who considered scattering by narrow-band waves as a random walk

Paper number 6A8489.
0148-0227/87/006A-8489$05.00

process occurring over many successive particle bounces. When interacting in the cyclotron resonance mode with incoherent electromagnetic disturbances, a trapped particle population is subjected to scatterings that are random in both direction and size. Hence the individual particles of the population undergo random walks in pitch angle and energy, and diffusion in velocity space results. This diffusion can be studied by calculating the incoherent diffusion coeficients and solving a Fokker-Planck equation [*Roberts*, 1966].

The diffusion approach is well justified for studying particle scattering by certain kinds of magnetospheric signals, for example, auroral VLF hiss or ELF plasmaspheric hiss, since such waves are indeed wide band and highly incoherent [*Muzzio*, 1971; *Gurnett and Frank*, 1972; *Thorne et al.*, 1973; *Laaspere and Hoffman*, 1976].

Recently, an approach to studying gyroresonant pitch angle scattering in the magnetosphere by coherent, narrow-band whistler mode waves has been developed, based on a test particle formulation [*Inan et al.*, 1978, 1982]. When a particle population encounters such coherent waves, the scatterings experienced by a particle are not random in direction or size. The individual particles of the population can be phase locked with the coherent signal over distances of many hundred wavelengths and may undergo large net pitch angle changes in a single encounter with the wave. It is therefore incorrect to assume that the particles execute a random walk in pitch angle during the course of one bounce period.

Examples of coherent magnetospheric whistler-mode signals are natural whistlers and discrete VLF chorus emissions [*Helliwell*, 1965], signals injected into the magnetosphere from ground based VLF transmitters [*Helliwell et al.*, 1964; *Helliwell and Katsufrakis*, 1974], discrete emissions triggered by whistlers as well as transmitter signals [*Helliwell*, 1983], and power line harmonic radiation [*Helliwell et al.*, 1975]. In this context, the word coherent is meant to describe waves having an "instantaneous" bandwidth (i.e., bandwidth measured in a time equal to one wave period) that is much smaller than the wave frequency. Recent discoveries of VLF chorus emissions in the magnetospheres of Jupiter and Saturn [*Scarf et al.*, 1981] and whistlers in the Jovian magnetosphere [*Gurnett et al.*, 1981] suggest that coherent waves are likely to exist in most magnetized plasmas. While our discussion in this paper is limited to whistler-mode waves interacting with electrons, it should be noted that magnetospheric waves propagating in other modes may exhibit coherent narrow-band behavior. Examples of such waves are some cases of electrostatic and electromagnetic ion cyclotron waves [*Temerin and Lysak*, 1984] and Pc micropulsations [*Jacobs*, 1970].

In this paper, we extend the test particle approach to interactions involving incoherent, relatively wide band whistler mode turbulence. The primary purpose is to quantitatively compare coherent and incoherent waves with respect to pitch angle scattering and resulting precipitation fluxes. Such a comparison should aid in determining the relative roles of different types of whistler mode waves in the dynamics of radiation belts. However, we note that an overall assessment of the respective contributions of, for example, whistlers and VLF hiss must be based on experimental data on the occurrence and spectral characteristics of these waves and on wave-induced precipitation events.

While much of the above mentioned theoretical work exclusively considered the pitch angle scattering of magnetospheric electrons, it should be noted that the general problem of coherent wave-particle interactions was also addressed by many other authors [*Brice*, 1964; *Helliwell*, 1967; *Dysthe*, 1971; *Nunn*, 1974; *Bud'ko et al.*, 1972; *Roux and Pellat*, 1978; *Karpman et al.*, 1975; *Vomvoridis and Denavit*, 1979; *Bell and Inan*, 1981; *Matsumoto and Omura*, 1981]. Most of these studies were targeted toward understanding the wave-growth and emission triggering aspects rather than pitch angle scattering; however, the underlying interaction physics and, for example, particle trajectories considered were the same. We also note that in considering the pitch angle scattering of electrons in the vicinity of the loss cone by coherent and incoherent waves we have not directly included the effects of feedback. Justification of this assumption for the purpose of computing the precipitation flux is given in earlier work [*Inan et al.*, 1978; *Bell and Inan*, 1981].

In the next section we discuss the application of a test particle formulation to the problem of gyroresonant pitch angle scattering in the magnetosphere. We then discuss the velocity space trajectories followed by electrons interacting with coherent versus incoherent waves and compare the mean square pitch angle scattering experienced by segments of the particle population under different conditions. A separate section on the comparison of test particle results with those expected using a diffusion analysis is followed by comparison of the computed precipitated flux for a monochromatic 400-ms-long wave packet and for a broadband (2-kHz bandwidth) signal of the same duration.

2. Test Particle Formulation of Gyroresonant Pitch Angle Scattering

The approach used in the test particle simulation is based on computing the full nonlinear trajectories of a large number of test particles and using these to infer the wave-induced perturbations of the trapped particle distribution and the resulting precipitation flux [*Inan et al.*, 1978]. The resonant encounters of the wave with particles (distributed over varying ranges of energy and pitch angle) as the wave packet propagates along the field line are taken into account. The contributions to the precipitated flux from interactions of particles entering the wave packet at different points along the field line are integrated, considering the travel times of the wave and particles to and from the scattering regions [*Inan et al.*, 1982]. The results are usually presented in terms of the precipitated energy flux as a function of time that would be observed at the ionosphere, and the energies of the particles that constitute the flux at different times during the wave-induced precipitation burst. The wave is generally assumed to originate either at 1000 km altitude, to represent the case of whistlers and man made waves injected from the ground, or near the magnetic equator, as would be expected in the case of triggered or spontaneous emissions such as VLF chorus or plasmaspheric hiss.

A number of important aspects of the magnetospheric problem are accounted for in the simulation. These include the full nonlinear equations of motion, the inhomogeneity of the medium for different models of the cold plasma distribution and the static magnetic field, the transient resonance encounter of the finite duration wave packet with particles at different points along the field line, a trapped electron distri-

bution function that can be arbitrarily specified in terms of its pitch angle and energy dependence, and the hemispherical asymmetry of the earth's magnetic field near the South Atlantic anomaly.

The test particle formulation for computing the pitch angle scattering due to coherent wave packets of finite duration has recently been used to study (1) the dependence of the temporal variation energy spectrum of the wave-induced precipitation flux upon various magnetospheric parameters [*Inan et al.*, 1982], (2) interactions involving relativistic particles [*Chang and Inan*, 1983*a*], and (3) interactions with waves exhibiting slowly varying frequency, such as whistlers and VLF emissions [*Chang et al.*, 1983]. The results obtained using the test particle formulation have allowed for comparison with experimental data from satellites and ground stations [*Chang and Inan*, 1983*b*; *Inan et al.*, 1985*a*]. In one case involving a satellite-based observation of precipitation induced by pulsed VLF transmissions, comparison of the theory and experiment revealed new aspects of the wave-induced precipitation process and provided "calibration" for the theoretical model [*Inan et al.*, 1985*b*]. More recently, the model has been used to predict the dynamic energy spectrum of the precipitation induced by short duration pulses as well as by lightning generated whistlers [*Chang and Inan*, 1985]. Such aspects of the wave-induced precipitation are now beginning to be measured [*Voss et al.*, 1984], and comparisons with model predictions are being made [*Inan et al.*, 1985*c*].

In contrast, much of the work on pitch angle diffusion of electrons due to interactions with incoherent waves has dealt with steady state conditions using simplified analytical descriptions of the medium and assuming limiting cases of either weak or strong diffusion [*Schulz and Lanzerotti*, 1974]. Electron diffusion rates are typically averaged over one particle bounce, and transient aspects, occurring on time scales of the order of one bounce period, are not addressed [*Roberts*, 1969]. The long term balance between sources and loss of particles and the implications of this in terms of the morphology of the radiation belts have been discussed using this approach [*Lyons et al.*, 1972]. However, such a formulation cannot easily be applied to recent experimental detection of bursts of precipitating energetic electrons that had apparently experienced single encounters with finite duration waves such as lightning-generated whistlers [*Voss et al.*, 1984; *Chang and Inan*, 1985].

In this paper we present a new technique for approximating an incoherent whistler-mode wave packet using random frequency modulation, and quantitatively compare pitch angle scattering due to finite duration coherent and incoherent wave packets propagating at $L = 4$.

Coherent and Incoherent Wave Packets

We first consider a monochromatic, circularly polarized, continuous whistler mode wave propagating along the static magnetic field $\mathbf{B}_0$. In the slowly varying magnetospheric medium, the WKB approximation [*Budden*, 1985] can be used and the wave magnetic field intensity can be expressed as

$$\mathbf{B}_w(z,t) = B_w(z)\left[\mathbf{a}_x \cos(\omega t - \int_{z_r}^{z} k(z)dz) + \mathbf{a}_y \sin(\omega t - \int_{z_r}^{z} k(z)dz)\right] \quad (1)$$

where z is the coordinate along $\mathbf{B}_0$, z_r is an arbitrary point of phase reference, ω is the angular wave frequency, $k(z)$ is the wave number and $\mathbf{a}_x$ and $\mathbf{a}_y$ are the unit vectors in the x and y directions, respectively. In the above, $B_w(z)$ is the slowly varying amplitude of the total field $\mathbf{B}_w(z,t)$ typically taken to be proportional to $[w_H(z)\mu(z)]^{1/2}$, where $\mu(z) = k(z)c/\omega$ is the local refractive index and $\omega_H(z)$ is the local electron gyrofrequency, and hence a measure of the cross sectional area of the VLF duct within which the wave is assumed to propagate [*Inan et al.*, 1982]. For whistler-mode propagation along $\mathbf{B}_0$ in a cold magnetoplasma, $k(z)$ is given approximately by

$$k \simeq \frac{\omega_p(z)}{c}\left[\frac{\omega}{\omega_H(z) - \omega}\right]^{1/2} \quad (2)$$

where c is the speed of light, and $\omega_p(z)$ is the local electron plasma frequency.

Using similar notation, a finite duration monochromatic whistler-mode wave packet can be described in terms of the x or y component of the wave magnetic field as

$$B_x(z,t) = B_w(z)\left[\cos(\omega t - \int_{z_r}^{z} k(z)dz)\right]\prod\left[\frac{t - t_f}{T_d}\right] \quad (3)$$

where t_f is the time when the wave front is at point z, T_d is the signal duration and $\prod(\varsigma)$ is the "gating" function defined as

$$\Pi(\varsigma) = 1 \qquad \varsigma \geq 0$$

$$\Pi(\varsigma) = 0 \qquad \varsigma < 0 \quad (4)$$

The other wave component B_y would have a similar form but is in phase quadrature with B_x as indicated in equation (1).

To represent an incoherent finite duration wave packet we use random frequency modulation. The wave packet is generated by randomly selecting the instantaneous frequency $\overline{\omega}_n$ of elementary pulses of length T, while keeping the phase continuous between successive pulses. The elementary pulse length is selected so that $T_d = NT$, where N is an integer. Using the previous notation, such a wave packet can be represented as

$$B_x(z,t) = B_w(z)\sum_{n=1}^{N}\left[\cos(\overline{\omega}_n t - \int_{z_r}^{z} k(z)dz)\right]\prod\left[\frac{t - t_f}{T}\right] \quad (5)$$

The instantaneous frequency of the elementary pulses is selected so that $\overline{\omega}_n = \omega_c + \omega_a r_n$, where ω_c is the center frequency, ω_a is the maximum frequency deviation and r_n is a random variable uniformly distributed over the range $-1 \leq r_n \leq 1$. If the power spectral density of the wave packet during each elementary pulse is to be kept constant, then $B_w(z)$ and $k(z)$ are implicit functions of wave frequency $\overline{\omega}_n$, the former being proportional to $[\mu(\omega)]^{1/2}$ as mentioned above, and the latter being a function of wave frequency ω as implied by (2). For the calculations reported in this paper we neglect this dependence and assume $B_w(z)$ to be independent of $\overline{\omega}_n$. This assumption is justified, since we consider a maximum 1-kHz deviation from a center frequency $f_c = \omega_c/2\pi$ of 5.5 kHz, which is approximately equal to the nose frequency at $L = 4$ [*Helliwell*, 1965].

The autocorrelation function and power spectral density of a random frequency modulated signal of the kind given

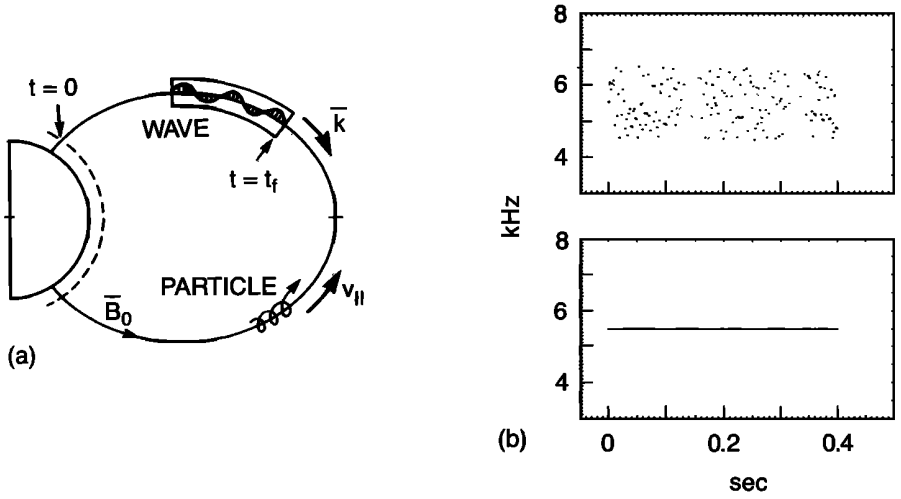

Fig. 1. (*a*) Schematic description of the wave–particle interaction phenomenology. (*b*) The frequency–time spectra of the incoherent and coherent wave packets used for comparison.

in (5) are discussed in the Appendix. It is shown that with appropriate choice of the parameters T, ω_a, ω_c, T_d, the spectral intensity can be made to approximate that of banded white noise, being nearly constant over a bandwidth of $\sim 2\omega_a$ centered around ω_c. However, the sample time domain waveforms described by (5) are of a specific form (i.e., non overlapping pulses) that in general represent a small subset of possible sample functions of a random process having a bandwidth of $\sim 2\omega_a$.

The use of random frequency modulation is a new technique for numerical simulation of noise-like waveforms having a banded power spectrum. Since the wave intensity is not allowed to fluctuate the simulation can be carried out using time step sizes determined by the characterisitc time of the wave particle interaction rather than the reciprocal of signal bandwidth. The same technique is also useful in experimentally generating noise-like signals and was recently used to simulate magnetospheric hiss in VLF wave-injection experiments using the Siple Station, Antarctica transmitter [*Helliwell, et al.*, 1986].

Equations of Motion

Once the wave structure is defined as above, the interaction of a distribution of particles with the wave packet is simulated by computing the velocity space trajectories of a representative number of test particles [*Inan et al.*, 1978]. This amounts to integrating the Lorentz force equation governing the particle motion over the region where significant interaction takes place, i.e., the region where

$$\omega + kv_{\parallel} \simeq \omega_H \tag{6}$$

where $v_{\parallel}$ is the component of the particle velocity parallel to the static magnetic field B_0.

For gyroresonant interactions of electrons with a whistler-mode wave propagating along the static magnetic field in the magnetosphere, the equations that govern the variation of the pitch angle α and velocity v of the particles can be written as

$$\dot{v} = \Omega_w \frac{\omega}{k} \sin\alpha \sin\phi \tag{7a}$$

$$\dot{\alpha} = -\Omega_w\left(1 + \frac{\omega}{kv}\cos\alpha\right)\sin\phi + \frac{v\sin\alpha}{\omega_H}\frac{\partial\omega_H}{\partial z} \tag{7b}$$

$$\dot{\phi} = \omega_H - \omega - kv\cos\alpha - \Omega_w\left(1 + \frac{\omega}{kv}\right)\frac{\cos\alpha}{\sin\alpha}\cos\phi \tag{7c}$$

where $\Omega_w = eB_w/m$, with e, and m being the electronic charge and mass respectively, ϕ is the complement of the angle between the wave magnetic field vector B_w and the electron's perpendicular velocity $v_\perp$, and v is the total particle velocity. Since $\omega < \omega_H$ for the whistler-mode, resonant interaction with electrons occurs when the wave and the particle travel in opposite directions, as indicated in Figure 1*a*.

In the inhomogeneous magnetospheric medium, $\omega_H = \omega_H(z)$ and $k = k[\omega_H(z), \omega_P(z)]$ vary along a given test particle's trajectory. For the cases discussed in this paper, we assume a centered dipole model for the earth's magnetic field and a diffusive equilibrium model for the background cold plasma density [*Angerami and Thomas*, 1964]. However, we note that the test particle formulation allows the use of any variation of these parameters, as demonstrated in previous applications of this technique [*Inan et al.*, 1983].

As the wave propagates along the field line it encounters a new distribution of particles at each point along its path. Each such distribution of particles is represented by a selected number of test particles, and the equations of motion (7) are integrated from the time the particles enter the wave packet until the time they exit from the wave tail. If the wave packet is much longer than typical interaction lengths, the motion equations are integrated only over the segment of the wave packet in which the condition (6) is valid (based on a separately established criterion) [*Inan et al.*, 1978].

Dispersion Effects

In previous test particle formulations of gyroresonant pitch angle scattering by parallel propagating whistler-mode waves, finite duration coherent wave packets were modeled as given in (3) above [*Inan et al.*, 1982; *Chang and Inan*, 1985]. For signals entering the magnetosphere at the ionosphere, the leading and trailing edges of the wave packet would be dispersed, so that by the time the wave arrives at the equator, the "gating" function $\prod(\zeta)$ representation given in (3) is not precisely correct. However, it can be shown that for the parameters used in this paper (i.e., $n_{eq} = 400$ cm^{-3} and $L = 4$), the spreading of a 3 to 5-

kHz wave pulse due to dispersion would be less than $\sim$ 20 ms [*Chang and Helliwell*, 1980]. Since the interaction times for individual particles are typically larger than $\sim$20 ms, this effect should be negligible as long as the pulse duration T_d is large enough to contain many cycles of the wave, i.e., $T_d >> 2\pi/\omega$. Based on this reasoning, dispersion effects have usually been neglected in earlier work involving gyroresonant scattering by coherent wave packets of > 200 ms duration [*Inan et al.*, 1982; *Chang and Inan*, 1985].

In contrast, dispersion effects along the propagation path of the type of incoherent randomly frequency-modulated signal described by (5) cannot be neglected. While the original wave packet consists of nonoverlapping T =1 ms pulses, dispersion would tend to distort the sharp edges of the pulses, typically by up to 10–20 ms (for example, as a result of propagation over half of the field line at $L = 4$). Furthermore, the difference in group travel time between pulses at the band edge frequencies for ω_a =1 kHz can be larger than the pulse duration (1 ms), so that the wave packet increasingly consists of overlapping and distorted pulses and thus cannot be represented by (5) above during its complete path along B_0. However, as discussed in the appendix, our use of (5) to represent an incoherent wave packet is not based on the time domain characteristics of the signal, but rather on the power spectral density of the random frequency-modulated wave packet, which can have a nearly flat distribution over a bandwidth of $\sim 2\omega_a$ centered around ω_c, depending upon the parameters T and ω_a. To the degree that the elementary pulse length $T << T_r$, where T_r is the typical duration of significant interaction or "resonance time," and is more precisely defined in the next section, the full extent of the power spectrum can be experienced by the resonant particles, and the representation of a broadband wave packet with (5) is valid regardless of the specifics of the time domain sample function.

In our calculations, the continual entry of new particles into the wave as its front advances is numerically approximated by using test particles that enter the packet at a finite set of points spaced by a distance less than the minimum instantaneous spatial extent of the wave packet along the field line [*Inan et al.*, 1982]. For wave packets with spatial extent comparable to the length of the field line, the spacing of the finite set of entry points is determined so as to accurately represent the differences in scattering efficiency as a function of geomagnetic latitude. For the parameters considered in this paper a mesh point spacing of $\sim 2^\circ$ in magnetic latitude was found to be satisfactory. Since dispersion effects would distort the wave packet significantly even over such a distance ($\sim$1000 km), we use the representation (5) with a different random number sequence for each wave front position. Particles encountering the wave packet at different positions along the field line then experience the same power spectral density but a different time domain pulse sequence, as would be the case for interactions involving an incoherent broadband wave packet.

Another consideration that needs to be addressed is the dispersion of the leading and trailing edges of the incoherent wave packet due to the variation of the group travel time with frequency across the signal bandwidth. The shape of the signal envelope can be assumed to remain unchanged as the signal propagates along the field line, as long as the duration of the wave packet (T_d) is significantly longer than the difference in group travel time at frequencies $\omega_c \pm \omega_a$. For $L = 4$ and with n_{eq} =400 cm^{-3}, as used in the following analysis, this condition is satisfied for pulses of $T_d = 400$ ms duration and bandwidth of $\sim$1-2 kHz centered on a frequency of $\sim$4–6 kHz.

3. PARTICLE TRAJECTORIES AND MEAN SQUARE SCATTERING

In this section we compare the pitch angle scattering induced by coherent versus incoherent waves in terms of (1) the velocity space trajectories of individual test particles, and (2) the mean square scattering of a set of particles distributed uniformly in Larmor phase ϕ.

'Equivalent' Coherent and Incoherent Wave Packets

For both the single particle scattering cases and the full distribution calculations reported in a later section we consider waves propagating at $L = 4$ where $n_{eq} = 400$ cm^{-3}. For comparison, we use two different wave packets of 400 ms duration (i.e, $T_d = 400$ ms), (1) a 5.5-kHz coherent wave as described by (3) with $\omega = 2\pi \times 5500$ rad s^{-1}, and (2) the other an incoherent wave packet as described by (5) with $\omega_c = 2\pi \times 5500$ rad s^{-1} and $\omega_a = 2\pi \times 1000$ rad s^{-1}. The two signals are shown in Figure 1*b* in a frequency-time format for a particular random frequency sequence $\overline{\omega}_n$.

In comparing the pitch angle scattering and the precipitated electron flux induced by the incoherent and coherent wave packets shown in Figure 1*b*, we note that the two signals are approximately 'equivalent' in the sense of having roughly the same wave power density. For the parameter values considered in this paper, the elementary pulse length T is greater than the wave period (i.e., $T > 2\pi/\overline{\omega}_n$), and both (3) and (5) represent waveforms that have the same peak-to-peak value at any point z. The signal power for any segment of duration T is then proportional to $\mu(\overline{\omega}_n)B_w^2(z)$. For $\omega_c = 2\pi \times 5500$ rad s^{-1} and $\omega_a = 2\pi \times 1000$ rad s^{-1}, $\mu(\omega_c \pm \omega_a)$ differs from $\mu(\omega_c)$ by only $\sim$ 4%, indicating that the wave power densities of the coherent and incoherent signals are roughly equal.

In terms of the power spectral density of the random frequency-modulated signal as given in the appendix, the "equivalence" of the incoherent and coherent signals can be expressed as

$$\int_0^\infty S(\omega)d\omega = B_w^2 \tag{8}$$

where $S(\omega)$ is the power spectral density of the random waveform described by (5) and B_w^2 represents the signal power for the coherent waveform given in (3). Although the limits of the above integral are given as 0 to ∞ to recognize the fact that the random frequency modulated signal has spectral energy at frequencies outside the range $\omega_c \pm \omega_a$, most of the wave power is confined to the range $\omega_c \pm 1.2\omega_a$ as shown in Figure A1 of the appendix.

In the following, we use an equatorial wave magnetic field intensity of $B_w = 1$ pT for both the coherent and incoherent signals as described by (3) and (5). The $B_w(z)$ at points other than the equator is related to that at the equator through the fact that $B_w(z)$ is proportional to $[\omega_H]^{1/2}$, as indicated above in connection with equation (1). At the equator for $B_w = 1$ pT, the power spectral density of the incoherent signal at the center frequency is $S(\omega_c) \simeq 5.6 \times 10^{-4}$ (pT)^2 Hz^{-1}, as shown in the appendix. If the power

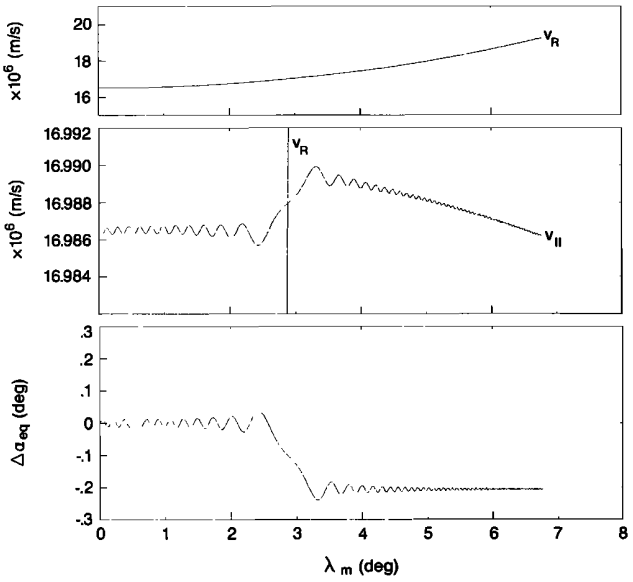

Fig. 2. The trajectory of a test particle in a coherent wave packet of 400 ms duration. All quantities are shown as a function of geomagnetic latitude λ_m. The particle encounters the wave front at the equator ($\lambda_m = 0°$). The top panel shows the resonance velocity v_R, the center panel the local particle parallel velocity $v_\parallel$ on an expanded scale, together with the v_R, and the lower panel the equatorial pitch angle change $\Delta\alpha_{eq}$. The initial equatorial pitch angle for the particle is $\alpha_{eq} = 5.5°$ and the initial Larmor phase is $\phi_0 = -90°$.

spectrum of the signal were completely flat over the range $\omega_c \pm \omega_a$ and zero outside, the spectral density would be $S(\omega_c) = S(\omega) = 5 \times 10^{-4}$ (pT)^2 Hz^{-1}, which is within 10% of the more accurately computed $S(\omega_c)$.

Particle Trajectories

For illustration of the particle trajectories we consider the particle population that encounters the front of the wave packet at the equator at time $t_f = 0$. From this population, we further select those particles having an equatorial parallel velocity and pitch angle of $v_{\parallel eq} \simeq 16,986$ km s^{-1}, $\alpha_{eq} = 5.5°$, for which the resonance condition (6) is precisely satisfied (for $\omega_a = 0$) at a point near $\sim 3°$ magnetic latitude on the same field line. This illustrates the more general case in which particles gradually approach the resonance region instead of being at or very near exact resonance at the time they encounter the wave front. Note that at $L \simeq 4$, $\alpha_{eq} = 5.5°$ corresponds to the equatorial loss cone angle, for a lowest mirror height of ~ 100 km. These selected particles represent only a very small fraction of the test particles that are typically used to simulate the distribution that encounters the wave at any point [*Inan et al.*, 1982]. This is further discussed in a later section.

The first example of the trajectory of a particle interacting with a coherent wave packet is shown in Figure 2. The top panel shows the variation with geomagnetic latitude of the resonance velocity $v_R = (\omega_H - \omega)/k$ obtained using (6). The center panel shows the same v_R on a much more expanded scale, together with the local parallel velocity $v_\parallel$ of the test particle evaluated via the numerical integration of the motion equations (7). We see that the particle undergoes rapid, noncumulative oscillations in $v_\parallel$ as it approaches its "resonance" point, signified by the crossing of $v_\parallel$ and v_R. Near the resonance point the particle experiences a net change in $v_\parallel$, and as it moves away it again experiences oscillatory perturbations, this time of increasing frequency and decreasing magnitude as the result of the increase of ω_H and $\dot{\phi}$ indicated in (7*c*). The slow downward variation of the local $v_\parallel$ is due to the adiabatic motion of the particle represented by the $\partial\omega_H/\partial z$ term in (7*b*).

The bottom panel in Figure 2 shows the change in the particle's equatorial pitch angle (i.e., the pitch angle referred to the equator) $\Delta\alpha_{eq}$. In the absence of the wave (i.e., $B_w = 0$) the equatorial pitch angle would not change, so that $\Delta\alpha_{eq} = 0$. The behavior of $\Delta\alpha_{eq}$ is similar to that of $v_\parallel$, showing increasing perturbations as the particle approaches resonance, followed by cumulative pitch angle change during the resonant encounter and decreasing perturbations after resonance, resulting in a net pitch angle change of $\Delta\alpha_{eq} \simeq -0.2°$. The termination point on the right of the curves in Figure 2 is the point where this particular test particle exits from the wave packet.

While Figure 2 illustrates the trajectory of a single particle having a particular initial Larmor phase of $\phi_0 = -90°$, Figure 3 uses the same format to show the variation of $v_\parallel$ and $\Delta\alpha_{eq}$ for 12 test particles, each having the same initial $v_{\parallel eq}$ and α_{eq} but a different initial phase ϕ_0 uniformly distributed in the range $-\pi \leq \phi \leq \pi$. The particles execute well defined orbits, and net scattering is distributed over the range $\Delta\alpha_{eq} \simeq -0.2°$ to $0.2°$. For cases such as this one, in which B_w is small enough so that phase trapping of the particle [*Inan et al.*, 1978] is not important, it can be shown [*Inan*, 1977] that the net scattering $\Delta\alpha_{eq}$ is proportional to $\sin\phi_0$, as is evident from Figure 3. This is further discussed in the next section.

The corresponding sample trajectories of the same particles in an incoherent wave packet are illustrated in Figures 4 and 5. Figure 4 shows the trajectory of the particle with $\phi_0 = -90°$. The format is the same as that of Figure 2

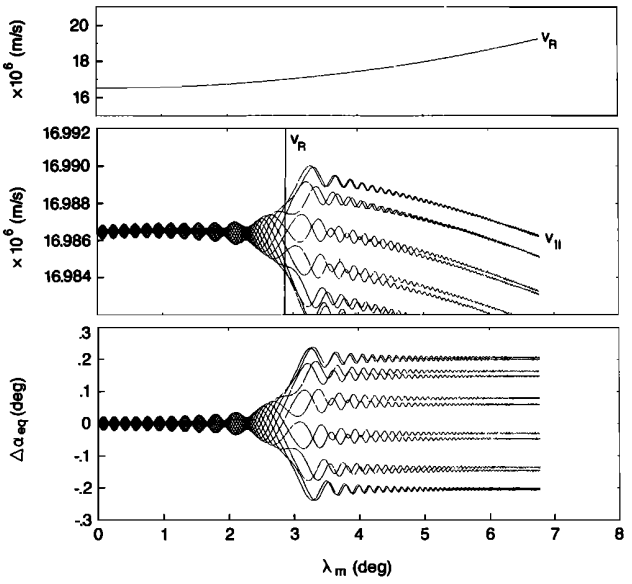

Fig. 3. The trajectories of 12 test particles interacting with a coherent wave. The particles are uniformly distributed in initial phase ϕ_0 and have the same initial parallel velocity. The formats of the three panels of this figure are identical to those of Figure 2.

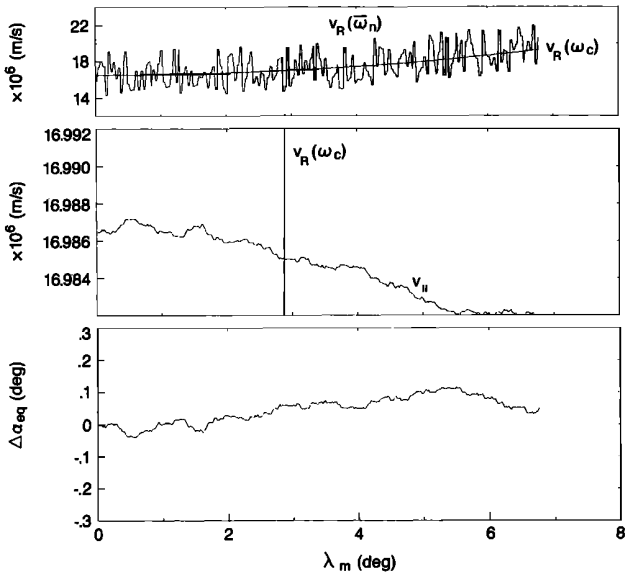

Fig. 4. The trajectory of a test particle in an incoherent wave packet of 400 ms duration. All quantities are shown as a function of geomagnetic latitude λ_m. The particle is assumed to encounter the wave front at the equator ($\lambda_m = 0°$). The top panel shows the resonance velocity $v_R(\bar{\omega}_n)$ corresponding to the random frequency sequence $\bar{\omega}_n$, and for reference the $v_R(\omega_c)$ corresponding to the band center frequency. The center panel shows the particle parallel velocity $v_\parallel$ together with the $v_R(\omega_c)$ on a significantly expanded scale, and the lower panel shows the equatorial pitch angle change $\Delta\alpha_{eq}$. The initial particle parameters are the same as those in Figure 2.

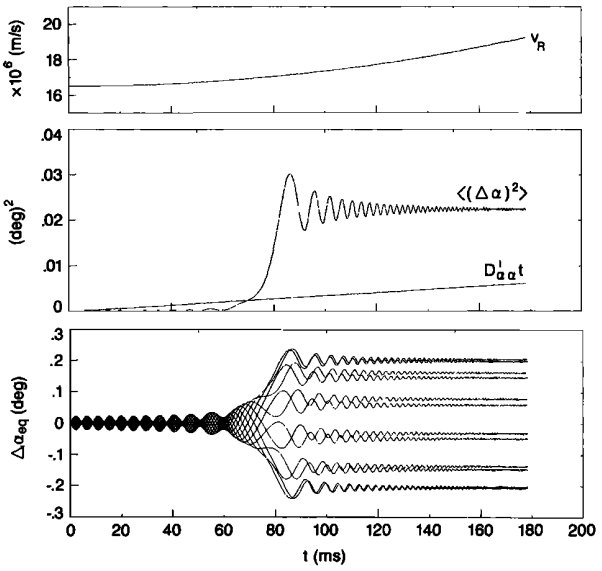

Fig. 6. Mean square scattering of 12 particles interacting with a coherent wave. The paremeters for this case are identical to those for Figure 2, with the top and bottom panels showing the same quantities plotted as a function of time t rather than geomagnetic latitude λ_m. Time $t = 0$ represents the time at which the particles encounter the wave front, in this case at the equator. The center panel shows the mean square scattering $\langle(\Delta\alpha)^2\rangle$, where the angular brackets indicate averaging over the initial phase ϕ_0. Also shown is the mean square scattering estimated using the incoherent diffusion rate $D^t_{\alpha\alpha}$ derived in section 4.

except for the top panel. In addition to the resonance velocity at the center frequency $v_R(\omega_c)$, this shows the resonance velocity $v_R(\bar{\omega}_n)$ corresponding to the random frequency sequence $\bar{\omega}_n$. A bandwidth in frequency of 2 kHz centered at ω_c results in a $\pm 15\%$ bandwidth in v_R centered at $v_R(\omega_c)$.

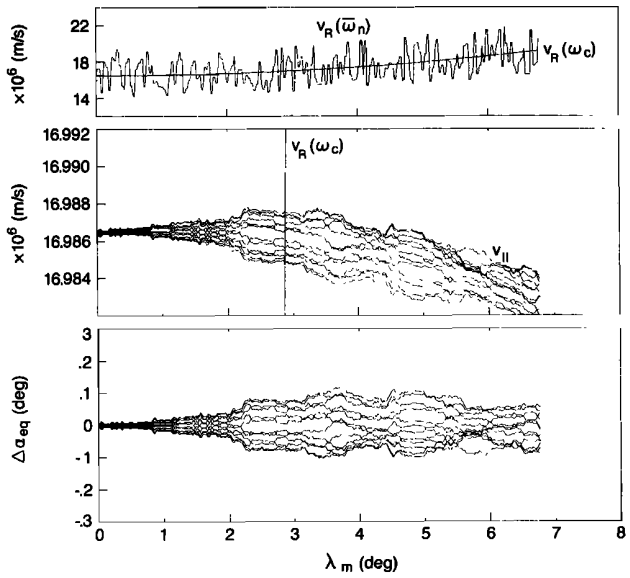

Fig. 5. The trajectories of 12 test particles interacting with an incoherent wave. The particles are uniformly distributed in initial phase ϕ_0 and have the same initial parallel velocity. The formats of the three panels of this figure are identical to those of Figure 4.

Figure 5 has the same format but shows the trajectories of 12 particles, uniformly distributed in initial phase ϕ_0.

Figures 4 and 5 show that in an incoherent wave the particles execute a random walk in $v_\parallel$ and α_{eq} superimposed on their adiabatic motion as illustrated by the slow background variation of $v_\parallel$ in the center panel. Note that scattering starts as soon as the particle enters the wave packet and continues until it exits from the wave tail. The fact that the interaction is not confined to the vicinity of the $v_\parallel \simeq v_R(\omega_c)$ crossing is expected, since the signal bandwidth expressed in terms of v_R encompasses $v_\parallel$ at all points shown, as indicated in the top panel of Figure 5.

Mean Square Scattering

We now discuss the mean square scattering, which is defined as the average over initial phase ϕ_0 of the square of the equatorial pitch angle change $\Delta\alpha_{eq}$, and is denoted as $\langle(\Delta\alpha_{eq})^2\rangle$. For a particle population uniformly distributed in initial phase ϕ_0 and having a given parallel velocity $v_\parallel$ and pitch angle α_{eq} , this quantity is a measure of the effective wave-induced pitch angle scattering for both coherent and incoherent interactions.

Figure 6 shows $\langle(\Delta\alpha_{eq})^2\rangle$ as a function of time, together with the individual particle trajectories for the case that was illustrated in Figure 3. Here $t = 0$ is taken to be the time at which the particles encounter the wave front at the equator. The formats of the top and bottom panels of Figure 6 are identical to those of Figure 3, except that the quantities are shown as a function of time instead of latitude. The particles exit from the wave tail at $t < 200$ ms, since for this case the wave group velocity is of the same order as the particle parallel velocity. Also shown for later reference in

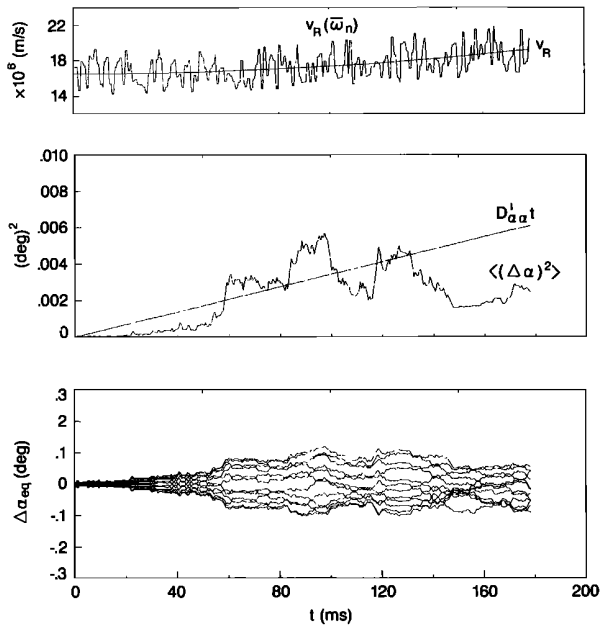

Fig. 7. Mean square scattering of 12 particles interacting with an incoherent wave. The parameters for this case are identical to those for Figure 5, with the top and bottom panels showing the same quantities plotted as a function of time t rather than geomagnetic latitude λ_m. Time $t = 0$ represents the time at which the particles encounter the wave front, in this case at the equator. The center panel shows the mean square scattering $\langle(\Delta\alpha)^2\rangle$, where the angular brackets indicate averaging over the initial phase ϕ_0. Also shown is the mean square scattering estimated using the incoherent diffusion rate $D^i_{\alpha\alpha}$ derived in section 4.

Figure 6 is the mean square scattering estimated using an incoherent diffusion rate $D^i_{\alpha\alpha}$ (see section 4).

Figure 6 shows that the mean square scattering of the 12 test particles is negligible until $t \simeq 60$ ms, at which time the particles' $v_\parallel$ are within $\sim 2\%$ of v_R as indicated from Figure 3. Significant cumulative scattering occurs until $t \simeq 120$ ms, when the particles are away from resonance by about the same percentage in $v_\parallel$. After this time, no significant net scattering occurs, although the $\langle(\Delta\alpha_{eq})^2\rangle$ exhibits oscillatory behavior with decreasing peak-to-peak amplitude and increasing frequency as the particles move further away from the resonance region. The "rate" of scattering within the $t \simeq 60$–85 ms time period is quite high in comparison with that expected from diffusion; this will be discussed further in the next section.

The mean square scattering due to interaction with an incoherent signal is illustrated in Figure 7. Here, we show $\langle(\Delta\alpha_{eq})^2\rangle$ as a function of time for the same conditions as those of Figure 5. The format of Figure 7 is identical to that of Figure 6, except for the vertical scale of the center panel, which is expanded by a factor of five. For the incoherent case the scattering commences as soon as the particles enter the wave packet at $t = 0$ and continues at roughly the same rate until they exit the wave's tail at $t \simeq 178$ ms. For the particular random frequency sequence $\bar{\omega}_n$ chosen here, the $\langle(\Delta\alpha_{eq})^2\rangle$ follows closely the scattering $D^i_{\alpha\alpha}t$ expected on the basis of diffusion. This comparison is further discussed in the next section in connection with Figure 10.

The results shown in Figures 2–7 are for particles that have the same initial parallel velocity $v_{\parallel eq} \simeq 16,986$ km s^{-1}, so that $v_\parallel \simeq v_R(\omega_c)$ at $\sim 3^\circ$ latitude. Figure 8 shows the resultant root mean square scatter $\sqrt{\langle(\Delta\alpha_{eq})^2\rangle}$ as a function of initial parallel velocity for the coherent case. Particles with different $v_{\parallel eq}$, ranging from 11,563 to 31,000 km s^{-1}, were injected into the wave at the equator, and the trajectories of 12 test particles uniformly distributed in ϕ_0 were computed. The resulting net $\sqrt{\langle(\Delta\alpha_{eq})^2\rangle}$ are shown in Figure 8. Particles with velocities less than $\sim 16,500$ km s^{-1} are not scattered, since their parallel velocity is significantly less than the equatorial resonant velocity v_R for a 5.5-kHz wave. This results from the transient nature of the interaction with a finite duration wave packet as considered here. The sharp peak at $v_{\parallel eq} \simeq 16,535$ km s^{-1} is due to the fact that these particles are very nearly resonant at the time they enter the wave packet and hence undergo large net scattering. Particles with higher parallel velocities approach resonance in a manner very similar to that shown in Figure 3, the resonance region being at increasingly higher latitudes for increasing $v_{\parallel eq}$. For particles having $v_{\parallel eq} > 18,795$ km s^{-1}, the $v_\parallel \simeq v_R$ crossing does not occur before the particles exit from the tail of the finite duration wave packet. Thus the net scattering $\sqrt{\langle(\Delta\alpha_{eq})^2\rangle}$ decreases significantly with increasing velocity and is negligible for $v_{\parallel eq} > 20,151$ km s^{-1}. In summary, Figure 8 indicates that for a particle population that encounters the wave front at a given location along the field line, significant scattering occurs in a well-defined range of parallel velocities.

Figure 9 shows the $\sqrt{\langle(\Delta\alpha_{eq})^2\rangle}$ versus $v_{\parallel eq}$ for the random scattering case, and for two different frequency sequences $\bar{\omega}_n$. As in Figure 8, all particles are taken to encounter the wave front at the equator, and the resultant scattering $\sqrt{\langle(\Delta\alpha_{eq})^2\rangle}$ is computed by evaluating the trajectories of 12 test particles at each $v_{\parallel eq}$. The scattering by the incoherent signal occurs over a wider range of parallel velocities, even though $\sqrt{\langle(\Delta\alpha_{eq})^2\rangle}$ at a given $v_{\parallel eq}$ is generally larger for the coherent case. As expected, the specific

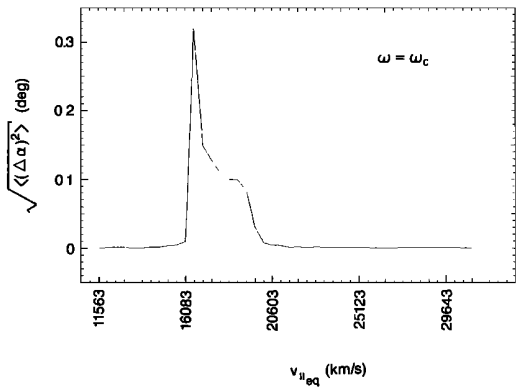

Fig. 8. Root mean square scattering induced by a coherent 400-ms-long wave packet at 5.5 kHz and having an equatorial wave magnetic field intensity of 1 pT, shown as a function of particle parallel velocity $v_{\parallel eq}$. All particles encounter the wave packet at the equator, and trajectories of 12 test particles at each $v_{\parallel eq}$ are computed to obtain the resultant root mean square scatter $\sqrt{\langle(\Delta\alpha)^2\rangle}$. The sharp peak at $v_{\parallel eq} \simeq 16,535$ km s^{-1} is due to the fact that these particles are very nearly resonant at the time they enter the wave packet and hence undergo large scattering.

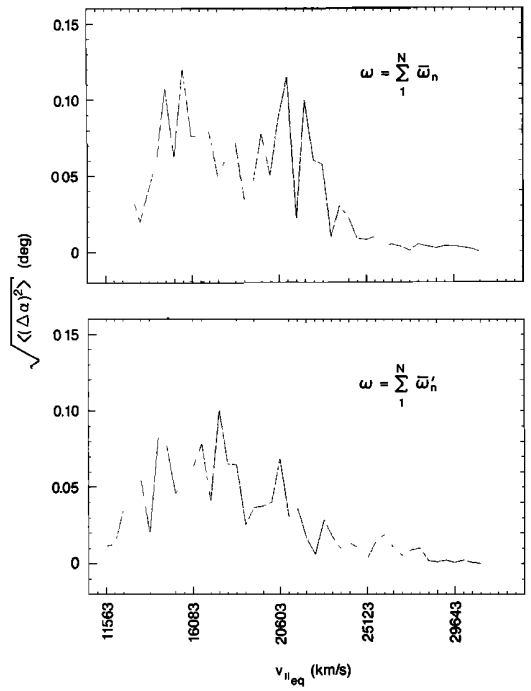

Fig. 9. Root mean square scattering induced by an incoherent wave packet, shown as a function of particle parallel velocity $v_{\parallel eq}$. All particles encounter the wave packet at the equator, and trajectories of 12 test particles at each $v_{\parallel eq}$ are computed to obtain the resultant root mean square scatter $\sqrt{\langle(\Delta\alpha)^2\rangle}$. The two panels show results for two different random frequency sequences $\bar{\omega}_n$.

variation of $\sqrt{\langle(\Delta\alpha_{eq})^2\rangle}$ with $v_{\parallel eq}$ is different for the two random sequences, but the general character is the same.

At the higher $v_{\parallel eq}$ end, scattering decreases with increasing velocity as the corresponding particles experience resonance within a decreasing fraction of the signal bandwidth. At the lower $v_{\parallel eq}$ end, a similar effect occurs as the velocity decreases.

Figures 8 and 9 quantitatively illustrate a result that is intuitively expected, that is, while the mean square pitch angle scatter is generally lower for incoherent interactions, the incoherent wave packet scatters a wider range of the particle population in velocity space. As demonstrated in a later section, this is the main reason why the overall precipitation energy flux induced by a short coherent wave packet is approximately the same as that of an incoherent wave packet having the same total wave power density.

4. Incoherent and Coherent 'Diffusion' Rates

In this section we present an analysis of our results in the context of a diffusion formulation that has in the past been used to study pitch angle scattering of electrons by broadband whistler-mode electromagnetic turbulence in the magnetosphere [*Roberts*, 1968; *Kennel and Petschek*, 1966]. We provide an approximate expression for a "diffusion" coefficient that can be used to describe the pitch angle scattering induced by coherent waves, and quantitatively compare this with diffusion rates that would be caused by incoherent waves. For this purpose, we use a simplified version of the motion equations (7)

$$\dot{\alpha} \simeq -\Omega_w\left(1 + \frac{\omega\cos^2\alpha}{kv_\parallel}\right)\sin\phi \tag{9a}$$

$$\dot{\phi} \simeq \omega_H - \omega - kv_\parallel \tag{9b}$$

The above are valid to first order under the conditions discussed in this paper, involving pitch angle scattering of particles in the vicinity of the loss cone at $L = 4$, with $n_{eq} = 400$ cm^{-3}, wave intensities of $B_w \simeq 1$ pT and for particles in the vicinity of the loss cone at $\alpha_{eq} \simeq 5.5°$.

Scattering by Incoherent Waves

For interactions involving an incoherent spectrum of waves, the diffusion coefficient is defined as [*Kennel and Petschek*, 1966]

$$D^i_{\alpha\alpha} \equiv \frac{\langle(\Delta\alpha)^2\rangle}{\Delta t} \tag{10}$$

where $\Delta\alpha$ is pitch angle change, the angular brackets denote an average over the wave spectrum, and Δt is the typical time for which the particle "remains in resonance" with a given wave spectral component at a frequency of $\omega_c \pm \Delta\omega/2$. An expression for Δt can be found by using a Taylor series expansion of $\dot{\phi}(\omega)$ around $\omega = \omega_c$ [*Roberts*, 1968], and adopting a phase change of $\Delta\phi \simeq \pi$ as the criterion for definition of the resonance duration. This gives

$$\Delta t \simeq \frac{2\pi}{\Delta\omega(1 + v_\parallel/v_g)} \tag{11}$$

where $v_g = d\omega/dk$ is the wave group velocity at $\omega = \omega_c$.

Using (11) and (9*a*) in (10), we find

$$D^i_{\alpha\alpha} \simeq \frac{\Omega_w^2}{\Delta\omega}\left(1 + \frac{\omega\cos^2\alpha}{kv_\parallel}\right)^2\left(\frac{\pi}{1 + v_\parallel/v_g}\right) \tag{12}$$

where $\Omega_w^2/\Delta\omega$ is proportional to the power spectral density at $\omega = \omega_c$ of the incoherent wave, i.e., $S(\omega_c)$ in the notation of the appendix.

Equation (12) represents a general version of the pitch angle diffusion coefficient that has been derived by other authors under limiting assumptions. For the case of $\omega << \omega_H$ (for which $v_\parallel >> v_g$) and for resonances involving high energy particles so that (9*a*) reduces to $\dot{\alpha} \simeq \Omega_w \sin\phi$, we can use $\Delta k \simeq \Delta\omega/v_g$ to rewrite the above expression as

$$D^i_{\alpha\alpha} \simeq \frac{\pi\Omega_w^2}{\Delta k v_\parallel} \tag{13}$$

which is identical to the pitch angle diffusion coefficient derived under similar assumptions by *Kennel and Petschek* [1966]. For interactions involving low energy particles, such as the case of protons and hydromagnetic waves, *Gendrin* [1968] has considered the more complete equation (9*a*) while still assuming $\omega << \omega_H$. While cases of $\omega < \omega_H$ but higher normalized frequency have been treated by *Roberts* [1968], the wave electric field effects, represented by the second term in (9*a*), were again neglected, since only relativistic electrons (i.e., $v_\parallel >> \omega/k$) were considered. For the cases treated in this paper, the general expression (12) must be used, since $\omega \simeq \omega_H/2$ and the resonant electron energies are low enough (0.3–10 keV) such that the particle parallel velocity $v_\parallel$ is comparable to the wave phase velocity $v_p = \omega/k$. A diffusion coefficient given by (12) was also used by *Helliwell et al.* [1975] in discussing pitch angle scattering by magnetospheric line radiation occurring in the 3 to 5-kHz range at $L \simeq 4$.

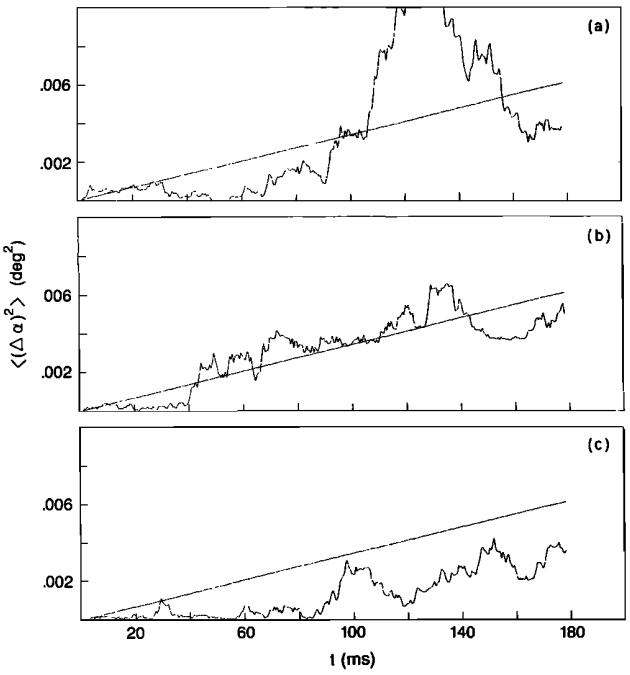

Fig. 10. Mean square scattering of 12 particles interacting with an incoherent wave. Time $t = 0$ represents the time at which the particles encounter the wave front, in this case at the equator. The three panels show the same quantity, in this case the mean square scattering $\langle(\Delta\alpha)^2\rangle$, for three different random frequency sequences $\overline{\omega}_n$. Also shown is the mean square scattering estimated using the incoherent diffusion rate $D^i_{\alpha\alpha}$ derived in section 4.

For the parameters of the case presented in Figures 3 and 6 of the previous section, the incoherent diffusion coefficient can be evaluated using $S(\omega_c) \simeq 5.6 \times 10^{-4}$ (pT)^2 Hz^{-1} (see appendix) in (12) as $D^i_{\alpha\alpha} \simeq 1.04 \times 10^{-5}$ s^{-1}. The mean square scatter $\langle(\Delta\alpha)^2\rangle = D^i_{\alpha\alpha}t$ based on this scattering rate is superimposed on Figure 6, showing that the results of the test particle analysis are consistent with those expected on the basis of a diffusion formulation.

The diffusion rate given by (12) represent the statistical average over the ensemble of all possible sample functions of the underlying stochastic process, in this case the random frequency sequence of $\overline{\omega}_n$. Thus $\langle(\Delta\alpha)^2\rangle$ computed for individual random frequency sequences is not, in general, expected to precisely match the average scattering of $D^i_{\alpha\alpha}t$. This is illustrated in Figure 10 by the $\langle(\Delta\alpha)^2\rangle$ computed with the test particle model for the case of Figure 7 but for different frequency sequences $\overline{\omega}_n$. The variation of $\langle(\Delta\alpha)^2\rangle$ for different sample functions can be substantially different from the average; however, even for the few samples shown in Figure 10, $D^i_{\alpha\alpha}t$ represents a reasonable "ensemble" average.

In the context of the above comparison, it should be noted that (12) represents a diffusion rate averaged over the wave spectrum, while in Figure 6, the angular brackets represent averaging over the initial Larmor phase ϕ_0. The statistical equivalence of the two averages can be seen by integrating (9*b*) to obtain the time variation of the phase ϕ as

$$\phi(t) \simeq \phi_u(t) - \Delta\omega(1 + \frac{v_\parallel}{v_g})t + \phi_0 = \phi_u(t) - \overline{\Delta\phi} \qquad (14)$$

where $\phi_u(t)$ is the unperturbed phase variation at frequency $\omega = \omega_c$ and ϕ_0 is the initial particle phase with respect to the wave. Since the pitch angle change $\Delta\alpha$ from (9*a*) is proportional to $\sin\phi$, the ensemble average $\langle(\Delta\alpha)^2\rangle$ is determined by the variance of the random variable $\overline{\phi(t)}$ which in turn is equal to the variance of the random variable $\overline{\Delta\phi}$ in (14). Since the variance of $\overline{\Delta\phi}$ should be the same for the case when ϕ_0 is known and $\Delta\omega$ is a uniformly distributed random variable and vice versa, the equivalence of the averages over ϕ_0 and the wave spectrum $\Delta\omega$ is evident.

Scattering by Coherent Waves

Gyroresonant pitch angle scattering by coherent waves is fundamentally different than that by incoherent waves, in that the individual particles of a population do not experience a random series of scatterings during their resonant encounter with a coherent wave [*Inan et al.*, 1978]. While this implies that a diffusion treatment is not suitable for analysis of coherent wave-induced scattering processes, an effective "diffusion" coefficient (or scattering rate) can be derived for the purpose of comparison with the diffusion coefficients computed above for incoherent waves.

For any particle with a given $v_\parallel$, the interaction with a coherent wave takes place in a region where the resonance condition (6) is satisfied. For low enough wave intensities such that phase trapping is not important, most of the wave-induced scattering occurs within a region centered around the exact resonance point and over which the phase ϕ would undergo a variation of $\Delta\phi < \pi$ radians in the absence of the wave [*Helliwell*, 1967; *Inan et al.*, 1978]. Using this criterion, and for particles with pitch angles near the loss cone, the interaction (or resonance) length L_r for resonant interaction around a point z near (but not necessarily at) the equator can be expressed as [*Inan et al.*, 1983]

$$L_r \simeq \left[\frac{16\pi v_R L^2 R_e^2}{9\omega_{Heq}}\right]^{1/3} \qquad (15)$$

where $R_e \simeq 6370$ km is the radius of the earth, v_R is the parallel resonant velocity at the point z, and ω_{Heq} is the gyrofrequency at the equator at this L-shell. Using (15), we can define $T_r \simeq L_r/v_R$ to be the 'resonance time', a quantity analogous to Δt used above for incoherent interactions. For the case shown in Figure 3 of the previous section, the interaction length is $L_r \simeq 895$ km, resulting in a resonance time of $T_r \simeq 52$ ms. This value is consistent with the result shown in Figure 6, where most of the mean square pitch angle scattering is seen to take place in a time of ~ 60 ms, from $t \simeq 60$ ms to $t \simeq 120$ ms after the particles' encounter with the wave front.

The "diffusion" coefficient for coherent wave-particle interactions near the geomagnetic equator can then be defined as

$$D^c_{\alpha\alpha} \equiv \frac{\langle(\Delta\alpha)^2\rangle}{T_r} \qquad (16)$$

where $\Delta\alpha$ is the net total pitch angle change for each particle and the angular brackets denote an average over the initial particle Larmor phase ϕ_0.

For coherent interactions, the net pitch angle change $\Delta\alpha$ must be evaluated by integrating (9*a*). Using linear theory, i.e., assuming that the wave intensity is low enough so that the particle perturbations can be computed using the unperturbed ($B_w = 0$) phase variation $\phi_u(t)$, it can be shown

that [*Inan*, 1977]

$$\Delta\alpha \simeq -\Omega_w \left(1 + \frac{\omega \cos^2 \alpha}{k v_\parallel}\right) \sin[\phi_0 + \beta] \sqrt{K_1^2 + K_2^2} \quad (17)$$

where $\beta = \tan^{-1}(K_2/K_1)$ and K_1 and K_2 are given by the following integrals:

$$K_1 = \int_{-\infty}^{\infty} \cos[F(t)]dt \qquad K_2 = \int_{-\infty}^{\infty} \sin[F(t)]dt$$

$$F(t) = \int_{-\infty}^{t} \dot{\phi}(\varsigma)d\varsigma$$

Note that $F(t)$ is the integral of equation (9*b*), which for an inhomogeneous medium involves the spatial variations of $\omega_H(z)$ and $k[\omega_p(z)]$. In practice, the above integrals for K_1 and K_2 need only be integrated over a limited range in the vicinity of "resonance" as is evident from the behavior shown in Figure 2 and as was discussed earlier in describing the numerical integration of the motion equations (7).

Averaging over initial phase ϕ_0 and substituting in (16) we obtain

$$D^c_{\alpha\alpha} \simeq \frac{\Omega_w^2 T_r}{2} \left(1 + \frac{\omega \cos^2 \alpha}{k v_\parallel}\right)^2 \left(K_1^2 + K_2^2\right) \quad (18)$$

as the coherent 'diffusion' coefficient.

To determine $\Delta\alpha$ and therefore $D^c_{\alpha\alpha}$ requires the proper evaluation of the integrals K_1 and K_2, which for an inhomogeneous medium cannot in general be done in closed form, even though approximate solutions based on a Taylor series expansion can be obtained using linear theory [*Ashour-Abdalla*, 1972]. In our case, we rely on the test particle simulation results, which involve the numerical solution of the complete equations (7), resulting in the computation of the particle trajectories and therefore $\Delta\alpha$. Sample solutions of $\alpha(t)$ for particles with initial phases of ϕ_0 and computed mean square scatterings $\langle(\Delta\alpha)^2\rangle$ averaged over the initial phase ϕ_0 were discussed in the previous section. These results can be used in (16) together with L_r (and thus T_r) from (15) to compute the pitch angle "diffusion" coefficient $D^c_{\alpha\alpha}$ for coherent interaction at different points along the field line. For the case discussed in Figures 3 and 6, the net mean square scattering is $\langle(\Delta\alpha)^2\rangle \simeq 0.025$ deg^2. Thus, the coherent diffusion coefficient as defined in (16) is $D^c_{\alpha\alpha} \simeq 1.46 \times 10^{-4}$ s^{-1}.

Comparison of Coherent and Incoherent Diffusion Rates

Using (18) and (12), the ratio of coherent to incoherent scattering rates can be written as

$$\frac{D^c_{\alpha\alpha}}{D^i_{\alpha\alpha}} \simeq \frac{W_B T_r}{2\pi} \left(1 + \frac{v_\parallel}{v_g}\right) \left(K_1^2 + K_2^2\right) \quad (19)$$

where we have taken the incoherent and coherent signal powers to be the same so that $(\Omega_w^2)^c \simeq W_B[(\Omega_w^2)^i/\Delta\omega]$, with W_B being the bandwidth of the incoherent wave packet. Note that for the random frequency-modulated signal used in this paper, $W_B \simeq 2\omega_a$ and $S(\omega_c) \simeq 2\pi(B_w^2)^i/\Delta\omega$ as discussed in an earlier subsection on the "equivalence" of the coherent and incoherent signals given in Figure 1*b*. The expression (19) should be taken to apply for resonances at points not far from the equator, where $v_\parallel$ is the resonant velocity v_R at frequency $\omega = \omega_c$ as obtained from (6).

Comparing the above obtained value of $D^c_{\alpha\alpha} \simeq 1.5 \times 10^{-4}$ s^{-1} with the $D^i_{\alpha\alpha}$ for a wave packet of bandwidth ~ 2 kHz, we find the ratio of the coherent and incoherent "diffusion" rates to be ~ 14. This is also evident from the center panel of Figure 6, which shows that within the interaction region the ratio of the slopes of the lines representing $\langle(\Delta\alpha)^2\rangle$ and $D^i_{\alpha\alpha}t$ is of the same order.

While the above indicates that the scattering rate is much higher for the coherent case, this result must be understood in view of the results of the previous section. For the incoherent case, the scattering takes place over a longer time period, essentially throughout the wave pulse as shown in Figure 7. For this case the incoherent interaction lasts for $\sim$ 178 ms, resulting in a mean square scattering of $\langle(\Delta\alpha)^2\rangle^i \simeq 0.007$ deg^2, which is only a factor of ~ 3.5 lower than $\langle(\Delta\alpha)^2\rangle^c$ and not a factor of ~ 14, as would be expected from the comparison of the local diffusion rates.

Discussion

The above results illustrate the differences and similarities between coherent and incoherent wave–particle interactions. While many aspects were evident from the test particle trajectories presented in the previous section, the analysis above relates these results to the predictions of a classical diffusion formulation. We see that even though the underlying particle trajectories are fundamentally different, an analogous "diffusion" coefficient can be defined for coherent wave-induced scattering. The computation of the value of this coefficient requires the integration of the motion equations (9), a task for which the test particle approach is well suited.

Once $D^c_{\alpha\alpha}$ is evaluated at different points along the field line, the total wave-induced scattering and the resulting precipitation flux due to the propagation of a wave packet from one hemisphere to another can in principle be evaluated. However, note that the scattering for each particle population identified with a $v_{\parallel eq}$ takes place over a limited region within the wave packet. All such details are accounted for in the test particle fomulation, which essentially amounts to computing the $D^c_{\alpha\alpha}$ at each point z and for each $v_{\parallel eq}$ along the wave propagation path and determining the fraction of the particle population that scatters into the loss cone.

In principle, a properly evaluated set of $D^c_{\alpha\alpha}$ can also be used in a Fokker–Planck formulation to determine the time evolution of the electron distribution function, as is commonly done for incoherent interactions [*Roberts*, 1968; *Gendrin*, 1968; *Lyons et al.*, 1972; *Davidson and Walt*, 1977]. Previously, coherent wave-induced scattering has not been studied from this point of view, although *Ashour-Abdalla* [1972] has analyzed the problem of scattering of particles by a coherent wave on successive bounces as a random walk, using a diffusion coefficient defined in a manner similar to (16), but with the denominator being the particle bounce period rather than the resonance time T_r.

5. Precipitation Flux Induced by Short Duration Wave Packets

In this section, we apply the formulation discussed above to estimate and quantitatively compare the precipitation flux induced by coherent and incoherent wave packets of 400 ms duration, which are assumed to enter the magnetosphere at $\sim$ 1000 km altitude. We consider the same wave packets

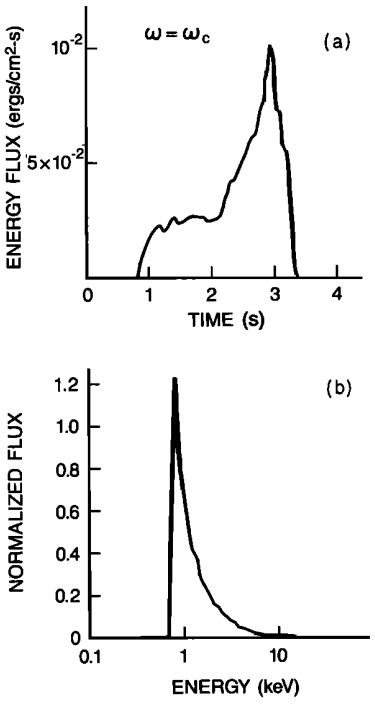

Fig. 11. Precipitation pulse induced by the 400-ms-long 5.5-kHz coherent wave packet with 1 pT magnetic field intensity: (*a*) integral energy flux versus time, (*b*) time-integrated flux versus energy, and (*c*) dynamic energy spectrum.

that are illustrated in Figure 1*b* and that were considered in the previous sections, namely a monochromatic 5.5-kHz signal of 1 pT intensity versus an incoherent signal having approximately the same total power and a bandwidth of ~ 2 kHz ($\omega_a = 2\pi \times 1000$ rad s^{-1}) centered around 5.5-kHz. The waves are assumed to be propagating at $L = 4$, where the equatorial cold plasma density was taken to be n_{eq}=400 cm^{-3}. The energetic particle distribution was assumed to be proportional to v^{-6}, except for an initially sharp loss cone. The differential energy spectrum for 1-keV particles with 90° pitch angle was taken to be 10^8 cm^{-2} s^{-1} sr^{-1} keV^{-1}.

Figure 11 shows the transient precipitation pulse induced by the 400-ms-long coherent wave packet, as it would be observed at 1000 km altitude in the same hemisphere as that in which the wave packet is initiated. The top panel shows the integral energy flux as a function of time, $t = 0$ being the time at which the wave packet enters the magnetosphere at 1000 km altitude. The time-integrated energy spectrum of the precipitation is shown in the bottom panel of Figure 11.

The corresponding results for the flux induced by the incoherent wave packet are shown in Figure 12. The temporal extent of the precipitation pulse for the incoherent case is broader and the energy spectrum indicates that the flux consists of particles having a wider range of particle energies, as was expected on the basis of the results of the previous sections. The peak intensities of the total energy flux for the incoherent and coherent cases are approximately the same, indicating that the less efficient scattering by the incoherent wave packet is compensated by the fact that a wider range of the particle population is affected. The relatively extended tail end of the precipitation pulse shown in the top panel of Figure 12 is due to the lower energy particles that are scattered by frequency components at frequencies $\omega > \omega_c$ and that arrive later due to their relatively low energy.

The above result, i.e., that the incoherent and coherent flux levels are approximately the same, would not be expected to hold in general. Although a tendency for such an equivalence is expected on qualitative grounds and on the basis of the results of the previous sections, the quantitative result is a consequence of the parameter values chosen, examples being the fact that the center frequency of 5.5 kHz is roughly equal to the nose frequency, that the particle distribution was assumed to vary smoothly with energy and that the wave magnetic field intensity of 1 pT is relatively low, so that the wave-particle interaction is substantially linear [*Inan et al.*, 1978].

For wave intensities large enough so that particles may become phase trapped in the wave's potential well, the coherent wave-induced scattering might result in higher precipitation fluxes since pitch angle changes of $\Delta\alpha_{eq}$ that can be a substantial fraction of the particle pitch angle α_{eq} [*Bell and Inan*, 1981]. For the parameters considered in this paper, such effects begin to become important for $B_w > 10$ pT. Most of the recent experimental findings of wave-induced particle precipitation events occurring at lower latitudes at $L < 3$ have been interpreted using wave magnetic field intensities below the trapping threshold [*Inan et al.*, 1985*a*].

We note an important implication of the above finding in terms of the use of theoretical models in the interpretation of experimental data. The tendency for the incoherent and coherent wave-induced fluxes to be approximately the same indicates that the resultant precipitation flux signatures are

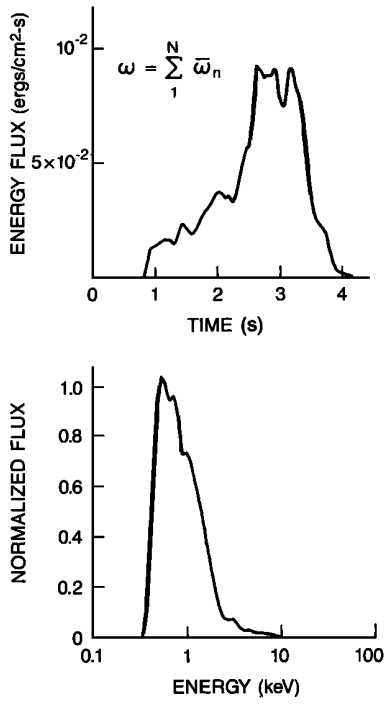

Fig. 12. Precipitation pulse induced by the 400-ms-long incoherent wave packet having ±1 kHz bandwidth centered around 5.5 kHz: (*a*) integral energy flux versus time, and (*b*) time-integrated flux versus energy.

not sensitive to the coherence of the observed waves and are mainly determined by first-order spectral characteristics such as wave frequency, frequency-time variation, propagation path and wave intensity. Thus the test particle model of gyroresonant wave-induced pitch angle scattering can be applied with increased confidence to a wide variety of experimental results, including precipitation events correlated with VLF noise bursts [*Dingle and Carpenter*, 1981]. Such events may either be studied by using an "equivalent" coherent wave packet or more directly by representing the noise burst as a random frequency-modulated signal.

6. Summary and Conclusions

We have compared gyroresonant pitch angle scattering in the magnetosphere due to interactions of energetic electrons with coherent and with incoherent whistler-mode waves. For this purpose, we made use of a test particle method for simulating the interaction of a particle population with a finite duration wave packet, a technique that has recently been utilized to study coherent wave-particle interactions [*Inan et al.*, 1982; *Chang and Inan*, 1985]. Incoherent wave packets were represented using random frequency modulation, thus allowing for calculations using time domain sample functions of broadband wave packets. This represents a new technique for numerical simulation of noiselike waveforms having a banded power spectrum. The fact that the wave intensity is not allowed to fluctuate means that the interaction with the incoherent signal can be modeled using time step sizes determined by the characteristic time of the wave-particle interaction (i.e., T_r) rather than the reciprocal of the signal bandwidth (i.e., $2\pi/W_B$), a significant saving in computation time.

Qualitatively, the trajectories followed by particles when interacting with incoherent waves represent a random walk in velocity space, while for coherent waves the particles' pitch angle and velocity vary in a well-defined manner. Quantitatively, for the cases studied in this paper, it was shown that the scattering (or "diffusion") rate within the resonance region for coherent interactions can be as much as a factor of 10–20 larger than that for incoherent waves. However, for a given particle population of given parallel velocity and encountering the wave packet at a given point along the field line, coherent wave scattering typically takes place over a limited region within the wave packet, while incoherent scattering can occur over a longer region. Thus, the resultant mean square scattering for incoherent interactions is found to be only a factor of 2–4 lower than that for coherent waves. Furthermore, an incoherent wave packet induces relatively small scatterings over a wider range of particle parallel velocities as compared to a coherent wave packet.

For an overall comparison of coherent versus incoherent wave-induced scattering and precipitation effects, we estimated the transient precipitation energy flux that would be induced by coherent and incoherent wave packets of 400 ms duration, propagating at $L = 4$. The peak energy flux resulting from the two different wave packets having the same power density was found to be approximately the same.

Results of the test particle analysis were also examined in the context of a diffusion formulation of gyroresonant pitch angle scattering [*Kennel and Petschek*, 1966; *Roberts*, 1968], and expressions for coherent and incoherent "diffusion" coefficients were derived and quantitatively compared. Through this comparision we have illustrated the differences and similarities between the classical diffusion analysis and test-particle-based modeling of gyroresonant wave-particle interactions in the time domain. It is intended that this presentation lead to a better understanding and appreciation of both approaches, and that it be helpful in the application of these techniques to studies of the roles of different kinds of waves in the dynamics and loss of radiation belt particles.

7. Appendix: Random Frequency Modulation

In simulating a quasi-random incoherent whistler-mode wave packet we have used a frequency-modulated signal in which the instantaneous frequency deviation from the carrier is taken to be a random number, uniformly distributed over the range of $-\omega_a$ to $+\omega_a$. In this appendix, we discuss the statistical characteristics of such a random frequency modulated signal $\mathbf{y}(t)$ and evaluate its power spectral density $S_{yy}(f)$.

Random Frequency Modulation

Consider a stochastic process $\mathbf{y}(t)$ to be the frequency-modulated signal given as

$$\mathbf{y}(t) = \cos(\omega_c t + \lambda\varphi(t) + \varphi_0) \qquad \varphi(t) = \int_0^t \mathbf{c}(\alpha)d\alpha$$

where ω_c is the carrier frequency, λ is the modulation index, and $\omega_c + \lambda\mathbf{c}(t)$ is the instantaneous frequency. The statistical autocorrelation function of the process $\mathbf{y}(t)$ can be shown to be given by [*Papoulis*, 1984]

$$R_{yy}(\tau) = \frac{1}{2}\mathrm{Re}[R_{xx}(\tau)e^{j\omega_c\tau}] \qquad \mathbf{x}(t) = e^{j\lambda\varphi}(t) \tag{A1}$$

If the process $\mathbf{c}(t)$ is stationary and the random variable φ_0 is independent of $\mathbf{c}(t)$, then the process $\mathbf{y}(t)$ is wide sense stationary with zero mean [*Papoulis*, 1984].

Woodward's Theorem

If the process $\mathbf{c}(t)$ is continuous and its first-order probability density function $f_c(c)$ is bounded, then for sufficiently large λ, the power spectral density $S_{yy}(\omega)$ of the process $\mathbf{y}(t)$ is given by

$$S_{yy}(\omega) \simeq \frac{\pi}{2\lambda}\left[f_c\left(\frac{\omega-\omega_0}{\lambda}\right) + f_c\left(\frac{-\omega-\omega_0}{\lambda}\right)\right]$$

Thus, if the probability density function of $\mathbf{c}(t)$ is chosen to be uniform over a given range $-\omega_a$ to $+\omega_a$, $S_{yy}(\omega)$ would be nearly flat over a similar range centered around the carrier frequency ω_0. This result is known as Woodward's theorem [*Woodward*, 1952].

Autocorrelation and Power Spectral Density for $\mathbf{w}(t)$

The incoherent waveform used in this paper (Figure 1*b*) was generated by using a random number generator for selecting the instantaneous frequency of elementary pulses of length T, while keeping the phase continuous between successive pulses. The pulse frequency was allowed to vary from $-\omega_a$ to $+\omega_a$, with equal probability of selecting any frequency in this range. The signal generated via this algorithm can be classified as a continuous-phase frequency shift

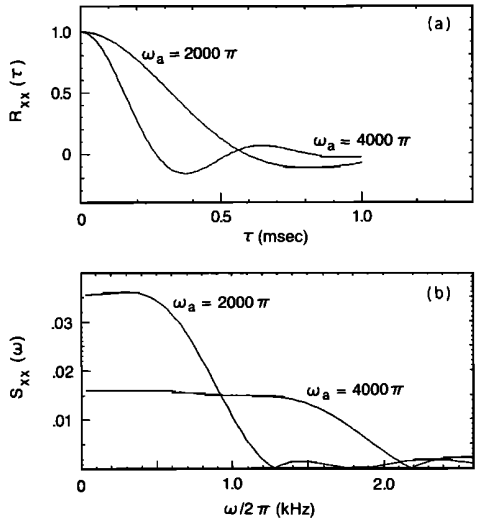

Figure A1. The (*a*) statistical autocorrelation function and (*b*) power spectral density of a random frequency-modulated signal shown for T=1 ms and $\omega_a = 2000\pi$ and 4000π rad s^{-1}. The functions shown correspond to the modulating process $\mathbf{x}(t)$. The power spectrum for $\mathbf{y}(t)$ is the same function shown in (Figure A1*b*) but centered around ω_c.

keying signal, in which the instantaneous frequency $\mathbf{c}(t)$ is a uniformly distributed random variable over the range $-\omega_a$ to $+\omega_a$. For the case in which the elementary pulse length T is an integral multiple of the period corresponding to the maximum frequency deviation ω_a, i.e., $T = 2\pi m/\omega_a$, with m an integer, the autocorrelation function of the process $\mathbf{x}(t)$ is given by [*Papoulis*, 1984]

$$R_{xx}(\tau) = \frac{1}{T}\int_0^\tau \Phi(\theta)\Phi(\tau-\theta)d\theta + (1-\frac{\tau}{T})\Phi(\tau) \qquad \tau \le T \tag{A2}$$

with $R_{xx}(\tau) = 0$ for $\tau > T$. In the above, $\Phi(\mu)$ is the characteristic function of the random variables $\mathbf{c}_n$. For the case in which these are uniformly distributed we have

$$\Phi(\mu) = \frac{\sin\omega\mu}{\omega\mu} \tag{A3}$$

Using (A2) and (A3), the power spectral density $S_{xx}(\omega)$ of the complex process $\mathbf{x}(t)$, defined as the Fourier transform of the statistical autocorrelation function $R_{xx}(\tau)$, can be found. The spectral density $S_{yy}(\omega)$ of the modulated carrier $\mathbf{y}(t)$ can be similarly found from $R_{yy}(\tau)$, which is related to $R_{xx}(\tau)$ through (A1).

Figure A1 shows plots of numerically computed $R_{xx}(\tau)$ and $S_{xx}(\omega)$ for $T = 1$ ms and for $\omega_a = 2\pi \times 2000$ and $\omega_a = 2\pi \times 1000$ rad s^{-1}. For both cases the spectral density is nearly flat at the band center and thus represents a good approximation of the spectrum for banded white noise. Furthermore, we see that the power spectrum is flat over a larger fraction of the signal bandwidth for the higher ω_a, as expected from Woodward's theorem discussed above.

Discussion

The spectra given in Figure A1 represent the power spectral density of the process $\mathbf{x}(t)$, which is assumed to be time-stationary. While the power spectral density of this process is similar to that of banded white noise, the sample functions of the random frequency modulated signal are of a specific form, i.e., nonoverlapping pulses that in general represent a small subset of possible sample waveforms of random process having a bandwidth of $\sim 2\omega_a$. To illustrate, this consider banded white noise having a $2\omega_a$ bandwidth. The minimum duration of elementary pulses in any one of the sample functions of such a process is $T_a = 2\pi/\omega$. Also, at any given time, more than one such elementary pulses can be present. On the other hand, the elementary pulse length for the random frequency-modulated signal is $T > T_a$ and furthermore, only one pulse is present at any given time. A sample function of the random frequency-modulated signal for $T = 1$ ms and $\omega_a = 2\pi \times 1000$ Hz is illustrated in Figure 1*b*.

The choice of the random frequency-modulated signal to represent an incoherent signal is motivated by the ease with which a time domain formulation such as the test particle model of *Inan et al.*[1982] can be adopted to treat this case. Since the signal consists of nonoverlapping pulses at randomly different frequencies, the trajectories of individual particles can be computed by integrating the equations of motion (7) in time, in the same manner as one does for a monochromatic signal, except for the use of $\overline{\omega_n}$ instead of ω.

In assessing the suitability of a random frequency-modu lated signal to represent for a broadband signal in the context of the gyroresonance wave-particle interaction, the elementary pulse length T must be compared with the typical duration of the resonance interaction between the wave and individual particles. Specifically, if the resonance time is given by T_r [*Helliwell and Inan*, 1982], then the condition $T_r >> T$ must be satisfied so that the full extent of the power spectral density of the waveform can be felt by the resonant particles. For the cases discussed in this paper, this condition is satisfied and thus our use of the random frequency signal is justified.

Acknowledgments. I thank my colleagues in the STAR Laboratory for many useful comments. The manuscript was prepared by K. Fletcher. This work was supported by the National Aeronautics and Space Administration under contract NGL-05-020-008.

The Editor thanks J. M. Cornwall and H. Matsumoto for their assistance in evaluating this paper.

REFERENCES

Angerami, J. J., and J. O. Thomas, Studies of planetary atmospheres, 1, The distribution of electrons and ions in the earth's exosphere, *J. Geophys. Res.*, *69*, 4537, 1964.

Ashour-Abdalla, M., Amplification of whistler waves in the magnetosphere, *Planet. Space Sci.*, *20*, 639, 1972.

Bell, T. F., and U. S. Inan, Transient nonlinear pitch angle scattering of energetic electrons by coherent VLF wave packets in the magnetosphere, *J. Geophys. Res.*, *86*, 9047, 1981.

Brice, N., Fundamentals of VLF emission generation mechanism, *J. Geophys. Res.*, *69*, 4515, 1964.

Budden, K. G., *The Propagation of Radio Waves*, Cambridge University, New York, 1985.

Bud'ko, N. I., V. I. Karpman, and O. A. Pokshtelov, Nonlinear theory of the monochromatic circularly polarized VLF and ULF waves in the magnetosphere, *Cosmic Electrodyn.*, *3*, 147, 1972.

Carpenter, D. L., and J. W. LaBelle, A study of whistlers correlated with bursts of electron precipitation near L=2, *J. Geophys. Res.*, *87*, 4427, 1982.

Chang, D. C. D., and R. A. Helliwell, VLF pulse propagation in the magnetosphere, *IEEE Trans. Antennas Propag.*, *AP-28*, 170, 1980.

Chang, H. C., and U. S. Inan, Quasi-relativistic electron precipitation due to interactions with coherent VLF waves in the magnetosphere, *J. Geophys. Res.*, *88*, 318, 1983*a*.

Chang, H. C., and U. S. Inan, A theoretical model study of observed correlations between whistler mode waves and energetic electron precipitation events in the magnetosphere, *J. Geophys. Res., 88*, 10053, 1983*b*.

Chang, H. C., and U. S. Inan, Test particle modeling of wave-induced energetic electron precipitation, *J. Geophys. Res., 90*, 6409, 1985.

Cornwall, J. M., Scattering of energetic trapped electrons by very-low-frequency waves, *J. Geophys. Res., 69*, 3075, 1964.

Cornwall, J. M., Micropulsations and the outer radiation zone, *J. Geophys. Res., 71*, 2185, 1966.

Cornwall, J. M., and Cocke, Theoretical simulation of micropulsations, *J. Geophys. Res., 72*, 2843, 1967.

Davidson, G. JT., and M. Walt, Loss cone distributions of radiation belt electrons, *J. Geophys. Res., 82*, 48, 1977.

Dingle, B., and D. L. Carpenter, Electron precipitation induced by VLF noise bursts at the plasmapause and detected at conjugate ground stations, *J. Geophys. Res., 86*, 4597, 1981.

Dungey, J. W., Loss of Van Allen electrons due to whistlers, *Planet. Space Sci., 11*, 591, 1963.

Dysthe, K. B., Some studies of triggered whistler emissions, *J. Geophys. Res., 76*, 6915, 1971.

Gendrin, R., Pitch angle diffusion of low energy protons due to gyroresonant interaction with hydromagnetic waves, *J. Atmos. Terr. Phys., 30*, 1313, 1968.

Goldberg, R. A., J. R. Barcus, L. C. Hale, and S. A. Curtis, Magnetospheric electron stimulation by lightning: Direct observation by rocket, *Eos Trans. AGU, 66*, 350, 1985.

Gurnett, D. A., and L. A. Frank, VLF hiss and related plasma observations in the polar magnetosphere, *J. Geophys. Res., 77*, 172, 1972.

Gurnett, D. A., F. L. Scarf, W. S. Kurth, R. R. Shaw, and R. L. Poynter, Determination of Jupiter's electron density profile from plasma wave observations, *J. Geophys. Res., 86*, 8199, 1981.

Helliwell, R. A., Whistlers and VLF emissions, *Research in Geophysics*, Vol. 1, *Sun, Upper Atmosphere, and Space*, MIT Press, Cambridge, Mass., 1964.

Helliwell, R. A., *Whistlers and Related Ionospheric Phenomena*, Stanford University Press, Stanford, Calif., 1965.

Helliwell, R. A., A theory of discrete VLF emissions from the magnetosphere, *J. Geophys. Res., 72*, 4773, 1967.

Helliwell, R. A., The structure of the plasmasphere on the basis of indirect measurements, in *Solar-Terrestrial Physics (1970)*; Part IV, edited by D. Dyer, D. Reidel, Hingham, Mass., 1972.

Helliwell, R. A., Controlled stimulation of VLF emissions from Siple Station, Antarctica, *Radio Sci., 18*(6), 801, 1983.

Helliwell, R. A., and U. S. Inan, VLF wave growth and discrete emission triggering in the magnetosphere: A feedback model, *J. Geophys. Res., 87*, 3537, 1982.

Helliwell, R. A., and J. P. Katsufrakis, VLF wave-injection experiments into the magnetosphere from Siple Station, Antarctica, *J. Geophys. Res., 79*, 2571, 1974.

Helliwell, R. A., J. P. Katsufrakis, and M. L. Trimpi, Whistler-induced amplitude perturbation in VLF propagation, *J. Geophys. Res., 78*, 4679, 1973.

Helliwell, R. A., J. P. Katsufrakis, T. F. Bell, and R. Raghuram, VLF line radiation in the earth's magnetosphere and its association with power system radiation, *J. Geophys. Res., 80*, 4249, 1975.

Helliwell, R. A., J. Katsufrakis, M. Trimpi, and N. Brice, Artificially stimulated very-low-frequency radiation from the ionosphere, *J. Geophys. Res., 69*, 2391, 1964.

Helliwell, R. A., S. B. Mende, J. H. Doolittle, W. C. Armstrong, and D. L. Carpenter, Correlations between λ4278 optical emissions and VLF wave events observed at $L \sim 4$ in the Antarctic, *J. Geophys. Res., 85*, 3360, 1980.

Helliwell, R. A., D. L. Carpenter, U. S. Inan, and J. P. Katsufrakis, Generation of band-limited VLF noise using the Siple transmitter: a model for magnetospheric hiss, *J.Geophys. Res.,91*, 4381, 1986.

Inan, U. S., Non-linear gyroresonant interactions of energetic particles and coherent VLF waves in the magnetosphere (Ph.D. thesis), *Tech. Rep. 3414-3*, Radiosci. Lab. Stanford Electron. Lab., Stanford Univ. Stanford, Calif., 1977.

Inan, U. S., T. F. Bell, and R. A. Helliwell, Nonlinear pitch angle scattering of energetic electrons by coherent VLF waves in the magnetosphere, *J. Geophys. Res., 83*, 3235, 1978.

Inan, U. S., T. F. Bell, and H. C. Chang, Particle precipitation induced by short-duration VLF wave growth and discrete emission triggering in the magnetosphere: A feedback model, *J. Geophys. Res., 87*, 6243, 1982.

Inan, U. S., R. A. Helliwell, and W. S. Kurth, Terrestrial versus jovian VLF chorus; a comparative study, *J. Geophys. Res., 88*, 6171, 1983.

Inan, U. S., H. C. Chang, R. A. Helliwell, W. L. Imhof, J. B. Reagan, and M. Walt, Precipitation of radiation belt electrons by man-made waves: A comparison between theory and measurement, *J. Geophys. Res., 90*(A1), 359, 1985*a*.

Inan, U. S., D. L. Carpenter, R. A. Helliwell, and J. P. Katsufrakis, Subionospheric VLF/LF phase perturbations produced by lightning-whistler induced particle precipitation, *J. Geophys. Res., 90*, 7457, 1985*b*.

Inan, U. S., R. A. Helliwell, D. L. Carpenter, H. D. Voss, and W. L. Imhof, A theoretical analysis of a lightning-induced electron precipitation event observed on the SEEP satellite, *Eos Trans. AGU, 66*, 1039, 1985.

Jacobs, J. A., *Geomagnetic Micropulsations*, Springer, New York, 1970.

Karpman, V. I., Ja. N. Istomin, and D. R. Shklyar, Effects of nonlinear interaction of monochromatic waves with resonant particles in the inhomogeneous plasma, *Phys. Scr., 11*, 278, 1975.

Kennel, C. F., and H. E. Petschek, Limit on stably trapped particle fluxes, *J. Geophys. Res., 71*, 1, 1966.

Laaspere, T., and R. A. Hoffman, New results on the correlation between low-energy electrons and auroral hiss, *J. Geophys. Res., 81*, 524, 1976.

Leyser, T., U. S. Inan, D. L. Carpenter, and M. L. Trimpi, Diurnal variation of burst precipitation effects on subionospheric VLF/LF signal propagation near L=2, *J. Geophys. Res., 89*, 9139, 1984.

Lohrey, B., and A. B. Kaiser, Whistler-induced anomalies in VLF propagation, *J. Geophys. Res., 84*, 5121, 1979.

Lyons, L. R., Comments on pitch-angle diffusion in the radiation belts, *J. Geophys. Res., 78*, 6793, 1973.

Lyons, L. R., Electron diffusion driven by magnetospheric electrostatic waves, *J. Geophys. Res., 79*, 575, 1974.

Lyons, L. R., R. M. Thorne, and C. F. Kennel, Electron pitch-angle diffusion driven by oblique whistler mode turbulence, *J. Plasma Phys., 6*, 589, 1971.

Lyons, L. R., R. M. Thorne, and C. F. Kennel, Pitch-angle diffusion of radiation belt electrons within the plasmasphere, *J. Geophys. Res., 77*, 3455, 1972.

Matsumoto, H., and Y. Omura, Cluster- and channel-effect phase bunching by whistler waves in a nonuniform geomagnetic field, *J. Geophys. Res., 86*, 799, 1981.

Muzzio, J. L. R., ELF propagations in the plasmasphere based on satellite observations of discrete and continuous forms, *Tech. Rep. 3439-2*, Radiosci. Lab., Stanford Electron. Lab., Stanford Univ. Stanford, Calif., 1971.

Nunn, D., A self-consistent theory of triggered VLF emissions, *Planet. Space Sci., 22*, 349, 1974.

Papoulis, A., *Probability, random variables, and stochastic processes*, McGraw-Hill, New York, 1984.

Roberts, C. S., Electron loss from the Van Allen zones due to pitch angle scattering by electromagnetic disturbances, in *Radiation Trapped in the Earth's Magnetic Field*, edited by B. M. McCormac, pp. 403–421, D. Reidel, Hingham, Mass., 1966.

Roberts, C. S., Cyclotron resonance and bounce resonance scattering of electrons trapped in the earth's magnetic field, in *Earth's Particles and Fields*, edited by B. M. McCormac,pp. 317–336, Reinholdt, New York, 1968.

Roberts, C. S., Pitch angle diffusion of electrons in the magnetosphere, *Rev. Geophys., 7*, 305, 1969.

Rosenberg, T. J., J. C. Siren, D. L. Matthews, K. Marthinsen, J. A. Holtet, A. Egeland, D. L. Carpenter, and R. A. Helliwell, Conjugacy of electron microbursts and VLF chorus, *J. Geophys. Res., 86*, 5819, 1981.

Roux, A., and R. Pellat, A theory of triggered emissions, *J. Geophys. Res., 83*, 1433, 1978.

Rycroft, M. J., Enhanced energetic electron intensities at 100 km altitude and a whistler propagating through the plasmasphere, *Planet. Space Sci., 21*, 239, 1973.

Scarf, F. L., D. A. Gurnett, and W. S. Kurth, Measurements of

plasma wave spectra in Jupiter's magnetosphere, *J. Geophys. Res., 86*, 8181, 1981.
Schulz, M., and L. J. Lanzerotti, *Particle Diffusion in the Radiation Belts*, Springer, New York, 1974.
Shawhan, S. D., Magnetospheric plasma wave research 1975-78, *Rev. Geophys. and Space Phys., 17*, 705, 1979.
Temerin, M., and R. L. Lysak, Electromagnetic ion cyclotron mode (ELF) waves generated by auroral electron precipitation, *J. Geophys. Res., 89*, 2849, 1984.
Thorne, R. M., E. J. Smith, R. K. Burton, and R. E. Holzer, Plasmaspheric hiss, *J. Geophys. Res., 78*, 1581, 1973.
Vomvoridis, J. L., and J. Denavit, Test particle correlation by a whistler wave in a nonuniform magnetic field, *Phys. Fluids, 22*, 367, 1979.
Voss, H. D., W. L. Imhof, J. Mobilia, E. E. Gaines, M. Walt, U. S. Inan, R. A. Helliwell, D. L. Carpenter, J. P. Katsufrakis, and H. C. Chang, Lightning-induced electron precipitation, *Nature, 312*, 740, 1984.
Woodward, P. M., The spectrum of random frequency modulation, *Telecommun. Res.*, 666, 1952.

U. S. Inan, STAR Laboratory, Stanford University, Stanford, CA 94305.

(Received March 27, 1986;
revised July 8, 1986;
accepted August 21, 1986.)